

Polynyas and Tidal Currents in the Canadian Arctic Archipelago

CHARLES G. HANNAH,^{1,2} FRÉDÉRIC DUPONT³ and MICHAEL DUNPHY¹

(Received 17 September 2007; accepted in revised form 14 April 2008)

ABSTRACT. A tidal model of the Canadian Arctic Archipelago was used to map the strength of the tidal currents, tidal mixing (h/U^3), and the vertical excursion associated with the tidal currents that drive water upslope and downslope. The hot spots in these quantities correspond to the location of many of the small polynyas in the archipelago, supporting the idea that the tidal currents make an important contribution to the dynamics of many of these recurring polynyas. The potential link with tidal mixing means that these locations may have enhanced plankton production in the summer.

Key words: Canadian Arctic Archipelago, polynyas, tidal currents, tidal mixing, tidal mixing fronts

RÉSUMÉ. Un modèle des marées de l'archipel Arctique canadien a servi à mapper la force des courants de marée, le mélange de marée (h/U^3) et l'excursion verticale associés aux courants de marée qui poussent l'eau en ascendant et en descendant. Les points chauds de ces quantités correspondent à l'emplacement d'un grand nombre des petites polynies de l'archipel, ce qui vient appuyer l'idée selon laquelle les courants de marée jouent un rôle important dans la dynamique d'un grand nombre de ces polynies récurrentes. Le lien susceptible d'exister avec le mélange de marée implique que la production de plancton à ces emplacements pourrait être rehaussée à l'été.

Mots clés : archipel Arctique canadien, polynies, courants de marée, mélange de marée, fronts de mélange de marée

Traduit pour la revue *Arctic* par Nicole Giguère.

INTRODUCTION

A polynya is a geographically fixed region of open water (or low average sea-ice thickness) that is isolated within thicker pack ice. Polynyas are an important component of both the physical and the biological systems in ice-covered seas (Smith and Barber, 2007), and they are widely distributed across the Canadian Arctic Archipelago (Fig. 1). From the physical point of view, polynyas are areas of enhanced air-sea fluxes in winter relative to the neighbouring ice-covered regions (Smith et al., 1983, 1990). From the biological perspective, polynyas that reliably occur each year are thought to be of particular ecological significance, especially for marine mammals and seabirds (Stirling, 1980; Stirling and Cleator, 1981).

Polynyas can continuously lose heat to the atmosphere without accumulating as much ice as the surrounding areas by several means. The two traditional categories of polynyas are latent heat polynyas, in which wind and currents drive away consolidated ice; and sensible heat polynyas, in which the heat flux from warmer subsurface waters slows or eliminates the formation of ice (Smith et al., 1990). The name “latent heat” refers to the latent heat of fusion released as the water is transformed into ice, and the name “sensible heat” refers to the oceanic heat required to keep the surface temperature above freezing. Williams et al. (2007) introduced a similar two-category classification based on the

mechanisms that remove or reduce the ice: mechanically forced (ice-divergence) and convectively forced (oceanic heat flux) polynyas. This classification is largely equivalent to the latent and sensible heat classification. Whichever classification is used, most polynyas are a mixture of the two categories. For example, the measured heat flux of 329 W m^{-2} at the Dundas Island polynya (Fig. 1, polynya No. 16) was shown to be 62% sensible heat and 38% latent heat (den Hartog et al., 1983).

Several secondary mechanisms can contribute to polynya maintenance: currents can sweep the newly formed (or frazil) ice out of the polynya and under the surrounding ice (den Hartog et al., 1983; Fig. 1); strong currents can increase heat conductance at the ice-water interface (Morse et al., 2006); and turbulence resulting from surface waves, strong currents, or both may inhibit the consolidation of frazil ice (Daly, 1994). Another important factor in polynya formation is shelter from drifting ice provided by coastlines, fast ice, or an ice bridge (Ingram et al., 2002; Williams et al., 2007). This shelter is important because no amount of latent or sensible heat flux can maintain a polynya against an influx of ice formed elsewhere.

The well-known North Water polynya in northern Baffin Bay (Fig. 1, polynya No. 21) is maintained primarily by latent heat or ice divergence (Ingram et al., 2002), as are the coastal leads that form when the winds and currents conspire to move the ice away from the coast. On the other

¹ Bedford Institute of Oceanography, Dartmouth, Nova Scotia B2Y 4A2, Canada

² Corresponding author: HannahC@mar.dfo-mpo.gc.ca

³ Department of Oceanography, Dalhousie University, Halifax, Nova Scotia B3H 4J1, Canada

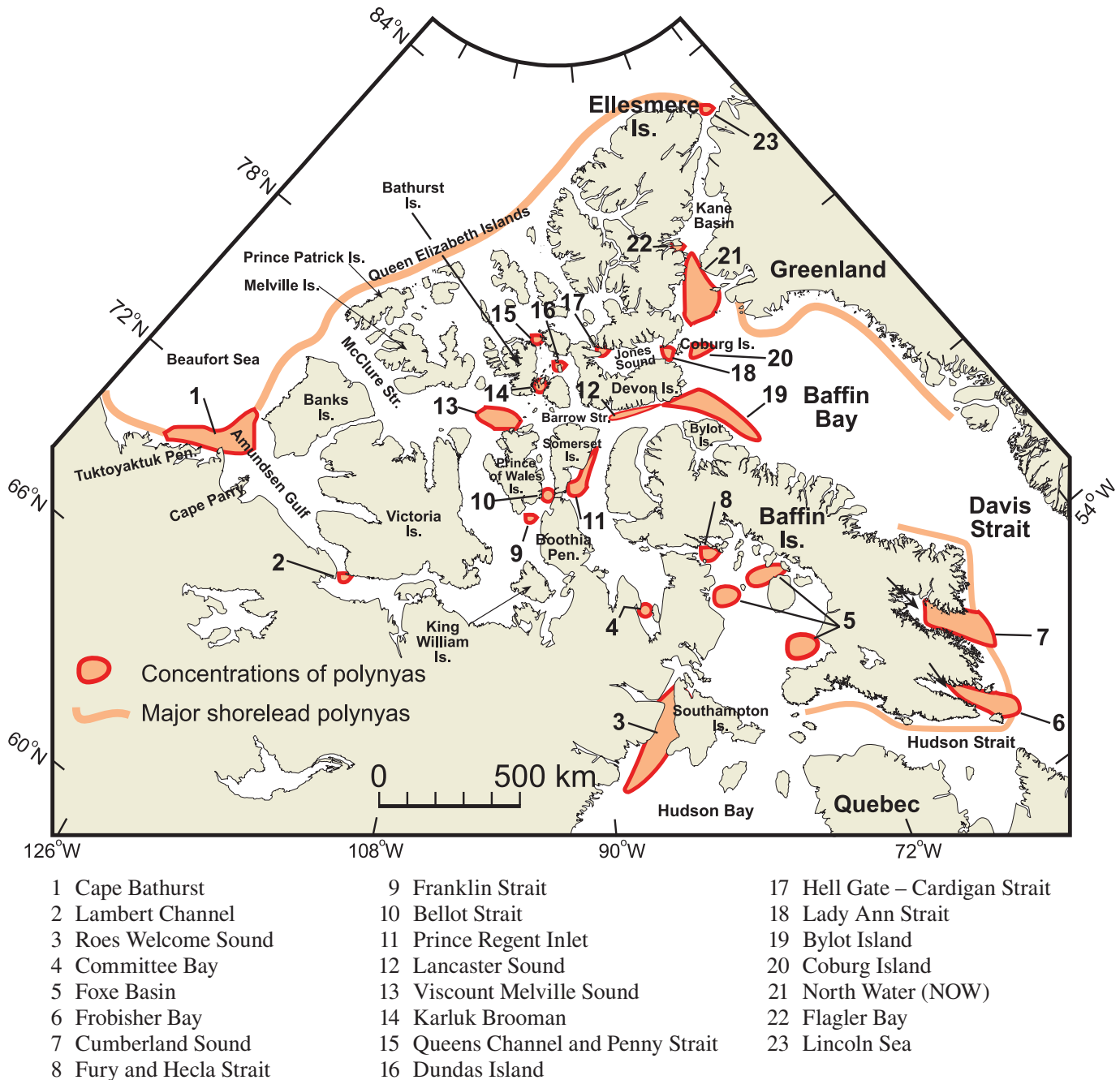


FIG. 1. A map of known polynyas in the Canadian Arctic, adapted from Barber and Massom (2007) and Stirling (1981). The Karluk Brooman polynyas were identified by Schledermann (1980) and Brown and Nettleship (1981).

hand, the Hell Gate polynya (Fig. 1, No. 17) and several others in the Canadian Arctic are thought to reflect an appreciable contribution of sensible heat (Topham et al., 1983; Smith et al., 1990) through the combination of a warm water reservoir at depth and strong tidal mixing. The importance of tidal mixing to ice dynamics is further supported by Saucier et al. (2004), who found that tidal mixing was crucial for the simulation of a stable seasonal cycle in an ice-ocean model of Hudson Bay.

The present study identifies areas in the Canadian Arctic Archipelago where tidal currents are likely to make important contributions to polynya formation and maintenance. A

simple conceptual model of tidal contribution to the sensible heat mechanism is shown in Figure 2. The tidal contribution requires three distinct features: a nearby source of warm water, a mechanism for getting the water from depth into shallower water, and strong tidal mixing to get the heat nearer to the surface. The transfer of heat from depth to the surface does not imply the existence of an unstable water column. In the Canadian Arctic, the stratification is dominated by salinity rather than temperature, and warmer water at depth is common (Melling, 2002). For the three secondary mechanisms mentioned previously, the only tidal factor is the strength of the currents.

As metrics of the potential tidal current contribution to polynya dynamics, we create maps of the tidal currents (U), the tidal mixing parameter h/U^3 (Simpson and Hunter, 1974; where h is the water depth), and the vertical excursion associated with the tidal currents that drive water upslope and downslope over a tidal period. The currents and water depths were taken from a depth-averaged tidal model of the Canadian Arctic Archipelago (Hannah et al., 2008). The analysis does not address the existence of a source of warm water.

In order to focus on the potential contributions from tidal currents, this analysis ignores currents, mixing, and upwelling due to the general circulation and wind forcing. Thus latent heat polynyas such as the North Water and Cape Bathurst polynyas should not be identified in the analysis.

The maps have potential uses beyond the interpretation of physical processes. In mid-latitude systems, the tidal mixing parameter h/U^3 has proven to be a robust measure of the potential for the vertical mixing associated with strong tidal currents to overcome the stratifying influence of the summertime surface heat flux (Simpson and Hunter, 1974; Garrett et al., 1978). The tidal mixing front is the transition zone from a stratified water column to a well-mixed one, and it is often a region of enhanced biological productivity (Backus and Bourne, 1987; Horne et al., 1989), especially in the summer.

METHODS

Tidal Model Overview

The implementation and validation of the tidal prediction system for the Canadian Arctic Archipelago is detailed in Hannah et al. (2008) and Dunphy et al. (2005). The model domain covers most of the region shown in Figure 1, including Baffin Bay and Davis Strait. The exception is that there is an open boundary in Fury and Hecla Strait (polynya No. 8), and the shelf regions to the south of the strait, such as Foxe Basin, Hudson Bay, and Hudson Strait, are not inside the model domain. The tidal model is MOG-2D (Carrière and Lyard, 2003), a two-dimensional finite element formulation with variable resolution. The horizontal resolution ranges from about 2 km in some coastal areas to 45 km in the open ocean.

The tidal elevation at the open boundaries was specified for the five major contributors to tidal variation (known as tidal constituents M_2 , N_2 , S_2 , K_1 , O_1). These constituents were estimated using the inverse modeling system that is part of the prediction system (details later in this section). The observed tidal constituents at 54 coastal locations were used in the assimilation, and the system was validated using 47 additional locations. The root-mean-square (rms) elevation error, averaged over all the stations, was about 13, 5, 7, 6, and 2 cm for M_2 , N_2 , S_2 , K_1 , and O_1 . This corresponds to a relative error of 13% for M_2 and 15–30% for the other four constituents. Overall the elevation errors are similar to those reported by Padman and Erofeeva (2004). The highlights of

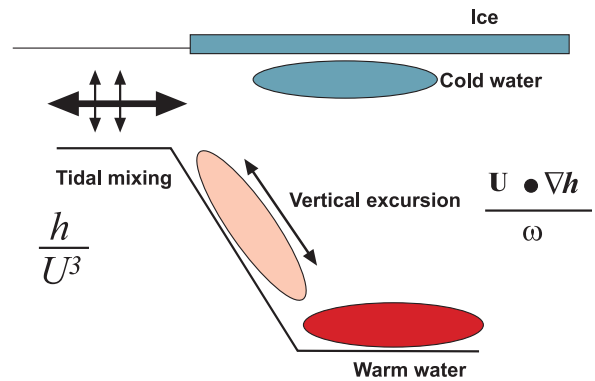


FIG. 2. Conceptual model of the contribution of tidal currents to the sensible heat mechanism. Symbols: h = water depth, ∇h = bathymetry gradient, ω = tidal frequency, U = tidal current, and h/U^3 = the tidal mixing parameter (Simpson and Hunter, 1974).

a regional evaluation of the solutions are provided in Appendix A.

Hannah et al. (2008) report a comparison of the modeled currents with the Acoustic Doppler Current Profiler (ADCP) data from five moorings across Barrow Strait (moorings SP1-5 in Fig. 3; Pettipas et al., 2006). Tidal analysis was done on the vertically averaged currents (from 10 m down to the bottom of the ADCP observations; 50 m at three of the four sites). The errors in the magnitude of the major axis currents for the two largest constituents, M_2 and K_1 , are 1–2 cm s^{-1} , which is small relative to the magnitude of the M_2 and K_1 major axis currents of 9–12 cm s^{-1} . The inclination of the ellipse is also reasonably well modeled, with errors less than about 10° . The magnitude of the minor axis (or eccentricity) is less well modeled, and the agreement with the tidal phase is poor for M_2 and reasonable for K_1 .

For further validation, we compared the M_2 and K_1 major axis currents at 17 locations in the archipelago (Figs. 3 and 4 and Appendix A). The major axis currents are a sensible validation metric since they dominate the calculation of the mean tidal current and U^3 . In locations with observations at more than one depth, the values were averaged to provide a value closer to depth-averaged. The results show reasonable correspondence between the modeled and observed currents. The largest currents and largest errors are at the three moorings in Cardigan Strait and Hell Gate (HM1–HM3), where the model underestimates the currents. In these two channels, the cross-channel structure represented by the model grid is very coarse, as there are only three grid points across the channel (one on each side and one down the middle).

These tidal solutions are available free of charge as part of the DFO WebTide application (OES-FOC, 2008) and can be used for detiding observations and other practical applications. For example, John Hughes Clarke (University of New Brunswick, pers. comm. 2007) uses the fields in an automated procedure to remove the tidal heights from the routine multibeam sonar measurements of water depth made by the CCG icebreaker *Amundsen* during cruises in the Canadian Arctic Archipelago. The detided results are then used to create maps by merging data from different cruises.

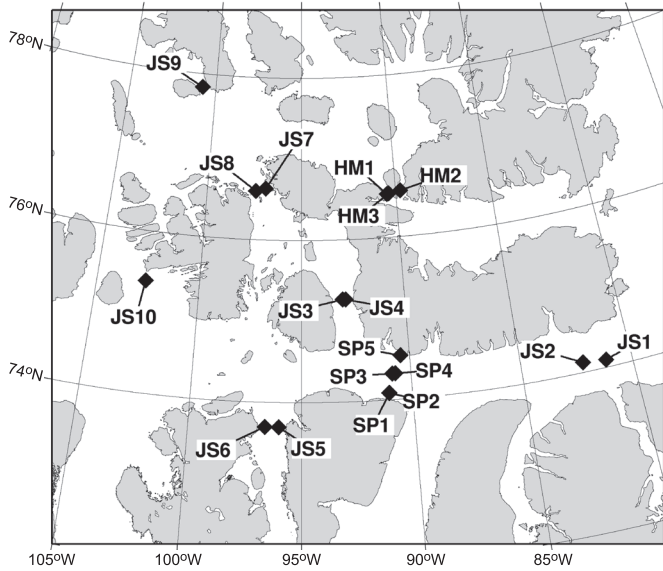


FIG. 3. Map showing current meter locations. See the Appendix for details of the mooring locations and data sources.

Derived Quantities

To assess the potential for the tidal currents to contribute to the secondary mechanisms, we computed the root-mean-square (rms) tidal currents over a 29-day period, where

$$rms(x) = \left[(1/N) \sum_{i=1}^N x_i^2 \right]^{1/2}$$

For h/U^3 we calculated $U^3 = \langle (u^2 + v^2)^{3/2} \rangle$ (the average over a 29-day period), where u and v are the time series of the north and east components of the tidal currents reconstructed from the five tidal constituents. We also considered maximum and minimum values of U^3 by computing maximum and minimum values of the daily averages of U^3 over the same 29-day period. The 29-day period is required to account for both fortnightly and monthly variations in the tidal currents. Given the large dynamic range of h/U^3 , the analysis is done using a log transform: $\lambda = \log_{10} h/U^3$.

To assess the potential of the tidal currents to move isotherms up and down in the water column, we estimated the vertical excursion due to the tidal currents over a sloping bottom. In two dimensions, this can be written:

$$\Delta z = |\nabla h| A / \omega \quad (1)$$

where $|\nabla h|$ is the magnitude of the bathymetric gradient, ω is the frequency, and $A = [(M \cos \theta)^2 + (m \sin \theta)^2]^{1/2}$, in which M is the magnitude of the major axis, m is the magnitude of the minor axis, and θ is the angle between the bathymetric gradient and the major axis of the currents. The excursion is calculated over one-quarter of the tidal cycle. The usual one-dimensional expression is recovered when

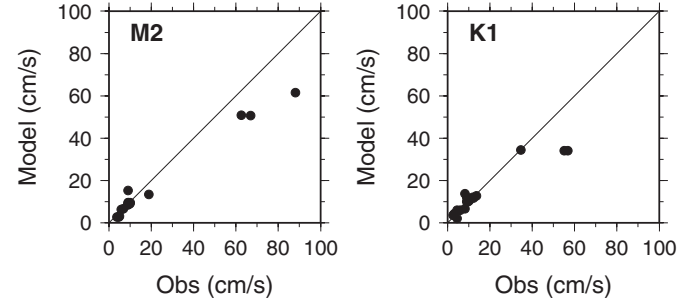


FIG. 4. Comparison of the observed and modeled major axis currents for M_2 and K_1 . Each dot represents the observed and modeled tidal current at a geographical location. If a dot falls below the diagonal line, then the modeled current is smaller than observed and if a dot falls above the line, then the modeled current is larger.

$\theta = 0$. The calculation was done separately for each of the two major tidal constituents in the Canadian Arctic Archipelago (M_2 and K_1), and the results were added together.

Tidal Model Details

The estimation of the tidal forcing at the open boundaries for the five major constituents (M_2 , N_2 , S_2 , K_1 , O_1) was done using the inverse modeling procedure that is part of the prediction system (Dupont et al., 2002, 2005). The step-by-step procedure is as follows: (1) Select a subset of the available observations for use in the assimilation system. The available observations should be distributed approximately evenly across the model domain. These observations are the initial values for the model-data misfit. (2) Use the model-data misfits as input to the inverse model and construct a new set of boundary conditions that reduces the model-data misfit. (3) Use the new boundary conditions to run the forward model to compute the tidal solutions and the model-data misfits. (4) Repeat steps 2 and 3 until the solution reaches the target error. (5) Evaluate the solutions against independent data.

The inverse model is the harmonic linear model TRUXTON (Lynch et al., 1998) modified to use spherical polar coordinates and to use a two-dimensional field of rms velocity from the forward model for the calculation of a spatially variable drag coefficient. The forward model is MOG-2D (Carrère and Lyard, 2003). Both models use the finite element formulation with variable resolution. TRUXTON is a three-dimensional model that requires consideration of the bottom friction and surface (ice) drag coefficients separately. MOG-2D is a depth-averaged model, and the friction term represents both the bottom and surface contributions, which are just added together. The bottom drag coefficient was set as $C_{\text{bot}} = 0.0025$. The surface drag associated with ice cover is discussed below.

TRUXTON requires three parameters as part of the inversion process: the expected error level (E_{rms}), the inverse square of the expected size of the boundary conditions (ω_0), and a dimensionless slope control (ω_1) that penalizes wiggly solutions along the boundary. For all inversions, $E_{\text{rms}} = 0.06$ m. For the first iteration, which captures the broad

features of each constituent, ω_0 was set to 10 m^{-2} for M_2 ; to 100 m^{-2} for N_2 , S_2 , and K_1 ; and to 1000 m^{-2} for O_1 , the weakest of all. Following the same philosophy, ω_1 was set to 10^{-3} for M_2 , N_2 , S_2 , and K_1 and to 10^{-4} for O_1 . For all other inversions, $\omega_1 = 10^{-4}$. For M_2 , $\omega_0 = 100 \text{ m}^{-2}$ and for the other constituents $\omega_0 = 1000 \text{ m}^{-2}$. The inversion process is described in detail by Dupont et al. (2002). The choice of inversion parameters was driven by the desire to have smooth solutions along the Arctic shelf. In preliminary experiments, the model showed a tendency to generate a series of amphidromes (locations where the tidal range is close to zero and the tide rotates about that location) along the Arctic shelf. In this case, the series of amphidromes was an unrealistic feature of the solution. We chose to suppress them and accept the less accurate simulation of the low-amplitude tides in the western Arctic.

The effect of the ice coverage was introduced as a quadratic friction term (analogous to bottom friction) where the drag coefficient C_{ice} was a linear function of the fractional ice coverage A : $C_{\text{ice}} = 0$ for $A < 0.5$, $C_{\text{ice}} = 1.8 \times 10^{-2}$ for $A = 1$ (Kliem and Greenberg, 2003). The value at $A = 1$, which is a fairly large value accounting for increased friction due to the keel effect in ridged ice, was taken from Tang and Fissel (1991). The rationale for setting the friction to zero for ice concentrations between 0 and 0.5 is that ice floes are believed to move freely along with the surface waters, exerting little drag. The friction value for smooth and undeformed landfast ice (connected to the shore) would be much smaller than the value used here. However, the process of landfast ice field formation includes interaction with the mobile offshore pack ice. Thus, the landfast ice often contains a series of ridges created during shearing and compressing episodes (Simon Prinsenberg, Bedford Institute of Oceanography, pers. comm. 2007). In general, the ice is a mixture of smooth and ridged ice in most of the archipelago, except for the fjords and the very nearshore (the first kilometre or so), both of which are under-resolved in this model.

The ice field used was the average of the observed coverage for September 1989 and January 1990. An (approximate) annual average was used for two reasons. First, in regions with strong spatial variability like the Canadian Arctic Archipelago, the assimilation scheme requires good spatial coverage. Reducing the data coverage by seasonally stratifying the data and eliminating constituents computed from records spanning several seasons would have resulted in poor solutions. Second, the observed changes in tidal amplitudes and phases between ice-free and ice-covered seasons are not large relative to the errors in the solutions. In Barrow Strait, for example, the largest observed changes are for M_2 and S_2 , which change by 3 to 6 cm (Prinsenberg and Hamilton, 2005). The amplitudes of O_1 , K_1 , and N_2 typically change by less than 2 cm. These changes are of the same order as the 6 cm expected error specified in the data assimilation scheme and less than the M_2 amplitude error of 12 cm obtained in the Barrow Strait region (Central region in the appendix). For these reasons, seasonally explicit solutions were not pursued. However, seasonal changes will need to be accounted for in efforts to further reduce the modeling errors.

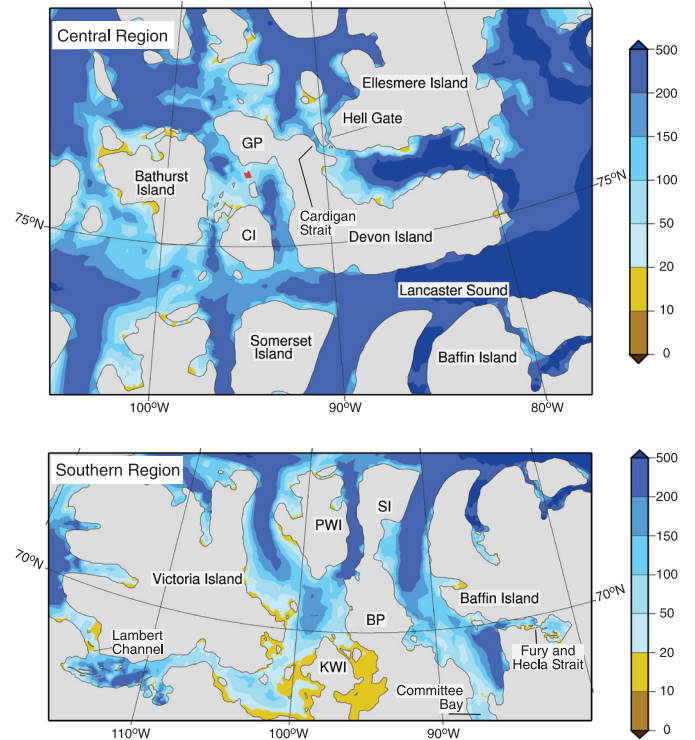


FIG. 5. Water depths (m) for the central (upper panel) and southern (lower panel) regions, using the coastline from the model grid. Abbreviations: BP - Boothia Peninsula; CI - Cornwallis Island; GP - Grinnell Peninsula; KWI - King William Island; PWI - Prince of Wales Island; SI - Somerset Island. Penny Strait and Queens Channel are between the Grinnell Peninsula (GP) and Bathurst Island. Dundas Island is the red dot due south of the GP label. Bellot Strait, which separates the Boothia Peninsula and Somerset Island, is not resolved in the model grid. It is located at the narrowest section of land between the BP and SI labels.

RESULTS

The results focus on two subregions of the Canadian Arctic Archipelago. The central region is centered on Devon Island (Fig. 5a) and includes polynyas at Hell Gate and Cardigan Strait, Queens Channel and Penny Strait, and Dundas Island. The southern region (Fig. 5b) includes polynyas at Lambert Channel, Committee Bay, Fury and Hecla Strait, and Bellot Strait.

The simulated tidal currents range from a few cm s^{-1} over large parts of the archipelago to 130 cm s^{-1} in Fury and Hecla Strait (Fig. 6). Tidal currents that exceed 30 cm s^{-1} are generally restricted to narrow channels and shallow areas, and most of these are regions with polynyas (e.g., Fury and Hecla Strait, Lambert Channel, Hell Gate, Cardigan Strait, Committee Bay, and the area near Dundas Island, which is due south of the Grinnell Peninsula). There are regions of strong currents on the west side of King William Island and one in the middle of the Gulf of Boothia (southeast of 70° N and 90° W), where there are no known polynyas.

The small values of $\lambda = \log_{10} h/U^3$ (strong mixing) are concentrated in a few, primarily constricted areas (Fig. 7). The results show $\lambda < 3$ in many areas of polynya formation (Fig. 1) documented by Stirling (1981), Smith and Rigby (1981), and Barber and Massom (2007), including Fury and

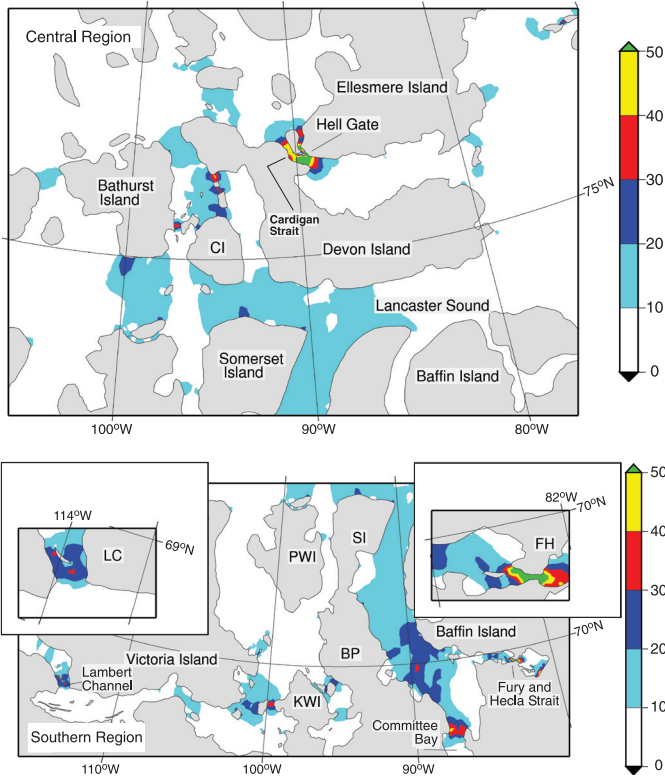


FIG. 6. The rms tidal currents (cm s^{-1}) for the central (upper) and southern (lower) regions. The inset in the upper left corner of the lower panel is Lambert Channel (LC) and the one in the upper right corner is Fury and Hecla Strait (FH). The maximum rms tidal currents are 130 cm s^{-1} in Fury and Hecla Strait (green) and 80 cm s^{-1} in Hell Gate and Cardigan Strait.

Hecla Strait, Hell Gate and Cardigan Strait, Dundas Island, Lambert Channel, Committee Bay, and Karluk Brooman. The North Water polynya and the coastal leads, both primarily of ice divergence (latent heat) origin, do not show up as areas with $\lambda < 3$. The Bellot Strait polynya between the Boothia Peninsula and Somerset Island is not represented. The results also show areas with $\lambda < 3$ around King William Island in the southern part of the archipelago, where there are no known polynyas.

The tidal currents exhibit significant fortnightly and monthly variability. At many locations, the changes in U^3 over the 29-day cycle result in changes in λ of 1 unit, which represents an order-of-magnitude change in the tidal dissipation. Near the time of minimum U^3 , the only areas with $\lambda < 3$ are in Fury and Hecla Strait and a few small areas in Hell Gate and Cardigan Strait (Fig. 8).

The vertical excursions in Figure 9 show the areas where the tidal currents have the greatest potential to move the isotherms up and down. The map highlights the importance of the narrow passages where the flow is forced to go over rather than around obstacles. The largest vertical excursions (in excess of 20 m) occur in Hell Gate, Cardigan Strait, Fury and Hecla Strait, and among the islands between Bathurst Island, Cornwallis Island and the Grinnell Peninsula (Devon Island). Other areas with potential vertical excursions in excess of 10 m include Lambert Channel, the Gulf of Boothia (to the east of the Boothia Peninsula) including

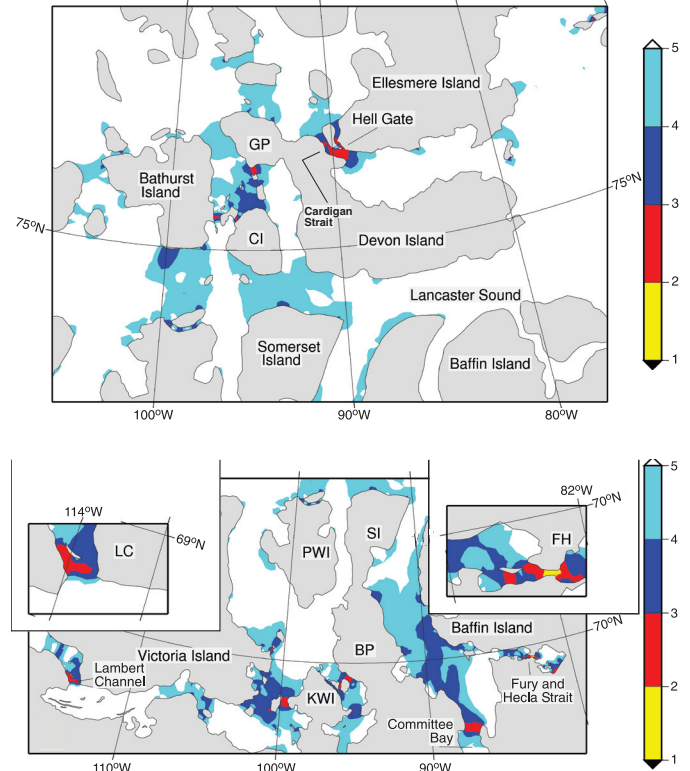


FIG. 7. The tidal mixing parameter $\lambda = \log_{10} h/U^3$ for the central and southern regions. Dundas Island and polynya are due south of the GP label. Penny Strait and Queens Channel and polynyas are between the Grinnell Peninsula (GP) and Bathurst Island.

Committee Bay, and the corners of many islands. The area around King William Island (in the southern archipelago) does not show any potential for large vertical excursions as the model bathymetry is quite flat. However, this result may be an artefact of the available bathymetry.

The area near the model boundary to the east of Fury and Hecla Strait shows large currents and small λ . This result is an artefact of the model solution near the boundary and will be ignored in the analysis that follows. Fortunately, the boundary does not contaminate the solution in Fury and Hecla Strait.

Indicators for Polynyas

The potential for the conceptual model in Figure 2 to provide a basis for predicting polynya locations is assessed using areas with $\lambda < 3$ (Fig. 7) and vertical excursions Δz greater than 10 m (Fig. 9). We call this value the sensible heat metric. The potential for the tidal currents (Fig. 6) to contribute to the secondary mechanisms (those directly related to currents) is assessed using areas with rms tidal currents greater than 30 cm s^{-1} . We call this value the velocity metric. The critical values for the metrics were chosen to define distinct geographical areas or hot spots consistent with the existence of polynyas at Hell Gate and Dundas Island, without restricting hot spots to those areas. The results are summarized in Table 1. Known polynyas identified by the sensible heat metric were also identified by the velocity metric.

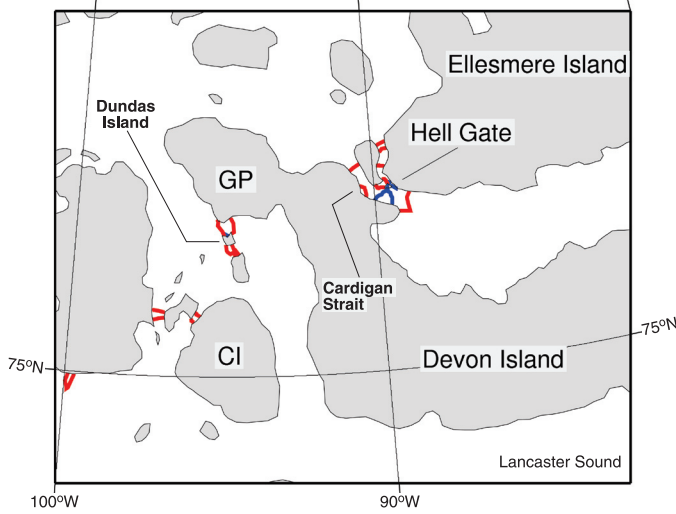


FIG. 8. Comparison of $\lambda = \log_{10}h/U^3$ for the maximum (U^3_{max}) and minimum (U^3_{min}) values of U^3 for part of the central region. The values of U^3_{max} and U^3_{min} were taken from 24-hour averages computed over a 29-day period. The contour value of $\lambda = 3$ is shown in red for U^3_{max} and blue for U^3_{min} .

DISCUSSION

Polynyas

The sensible heat and velocity metrics do a good job of identifying locations where tidal currents are likely to make an important contribution to polynya dynamics (Table 1), despite the many limitations of the pragmatic mapping approach. The polynyas at Hell Gate and Cardigan Strait and Dundas Island have been previously identified as ones where tidal mixing makes a substantial contribution to the sensible heat flux (Topham et al., 1983; Smith et al., 1990). The Karluk Brooman polynyas between Cornwallis Island and Bathurst Island were not identified by Stirling (1981) or Barber and Massom (2007). Their apparent presence was considered a failure of the model until we learned of their existence from Schledermann (1980) and Brown and Nettleship (1981). The lead that develops into the Committee Bay polynya is not well understood. Nevertheless, it is encouraging that both Smith and Rigby (1991) and Barber and Massom (2007) indicate that winds and tidal currents are important parts of the dynamics. Barber and Massom (2007) do not provide a definitive identification of the polynya type for the Lambert Channel polynya; however, Smith and Rigby (1981) comment on the many shoal areas and the heavy tidal rips in the channel.

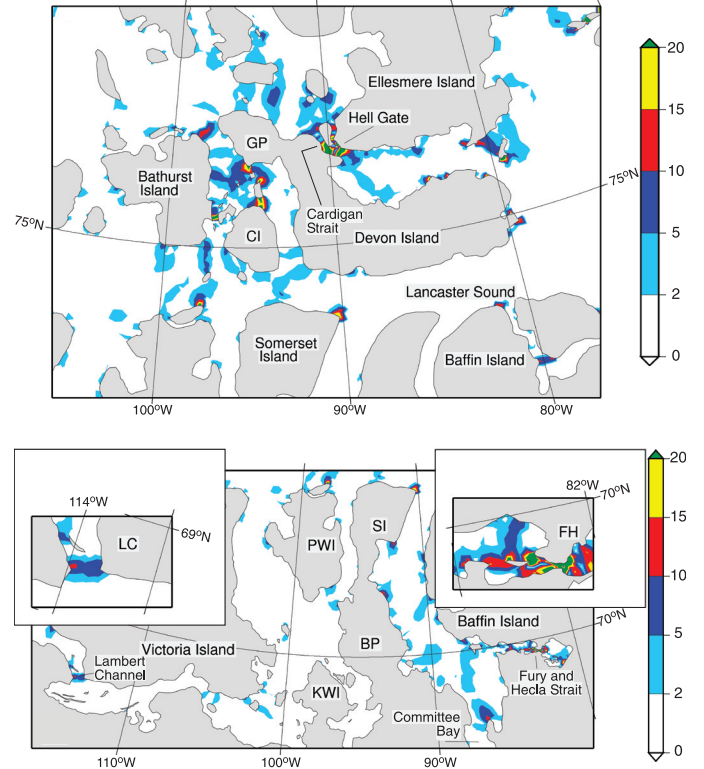


FIG. 9. The vertical excursion (m) due to the M_2 and K_1 tides for the central and southern regions. This is a simple measure of the potential for the tidal currents to move the isotherms up and down in the water column. A value of 10 m does not necessarily mean that the isotherms have a 10 m vertical motion.

Several known polynyas are not identified by either metric (Table 1). In some cases we expect that increased horizontal resolution in the model so that small islands and other small-scale features are resolved will increase the modeled tidal currents in these locations. For example, the narrow Bellot Strait is not resolved in our model, and the very large tidal currents associated with the strait (Table 4.2.1 in Stro-nach et al., 1987) are missing. Preliminary simulations with a crude representation of Bellot Strait show strong tidal currents that would satisfy both metrics. These currents may play a role for both the Bellot Strait and the Prince Regent Inlet polynyas. Smith and Rigby (1981) report that the very small Franklin Strait polynya (less than 2 km wide) is associated with a group of small islands (the Tasmania Islands). These islands are not represented in the tidal model. In Penny Strait and Queens Channel, the simulated currents are relatively weak. We note that the model grid has only four

TABLE 1. A summary assessment of the potential for identifying known polynya locations using the sensible heat and velocity metrics. The justification for the polynyas listed under “Needs further tidal modeling” is given in the text. The superscript numbers following the polynya names correspond to the numbering in Figure 1.

Polynya Metric Category	Polynyas
Sensible heat metric and Velocity metric	Lambert Channel, ² Committee Bay, ⁴ Fury and Hecla Strait, ⁸ Dundas Island, ¹⁶ Hell Gate–Cardigan Strait, ¹⁷ Karluk Brooman polynyas ¹⁴
Needs further tidal modeling	Franklin Strait, ⁹ Bellot Strait, ¹⁰ Prince Regent Inlet, ¹¹ Queens Channel and Penny Strait ¹⁵
Unlikely to be related to tidal currents	Lancaster Sound, ¹² Viscount Melville Sound, ¹³ Lady Ann Strait, ¹⁸ Coburg Island, ²⁰ Bylot Island ¹⁹

or five nodes across Penny Strait between Bathurst Island and the Grinnell Peninsula. This number may suffice for calculating the tidal heights, but it is not sufficient to resolve the small islands and other small-scale bathymetric features that may lead to larger tidal currents. Thus we cannot make firm conclusions about the role of tidal currents in the Penny Strait and Queens Channel polynyas. Further tidal modeling is needed to assess whether we have correctly explained why the model did not identify these polynyas.

The area around King William Island contains one hot spot in the velocity metric, but not in the sensible heat metric. This is an area with $\lambda < 3$ but where the vertical excursions are small. The lack of observed polynyas may be due to the limited vertical excursions and the lack of a deep basin to act as a reservoir of warm water (Fig. 5b). Table 1 also lists several polynyas that were not identified by either metric, in locations where we would not expect additional tidal modeling to change the results.

In summary, the two metrics identified locations where the tidal currents were previously known to be important, locations where there are known polynyas whose dynamics have not been well established, and one location where a known polynya was not part of our initial set. The metrics have also identified several regions where the tidal current modeling needs to be improved. Finally, given that the tidal currents were not expected to contribute to all polynyas, it is important that there are many polynyas whose locations are not indicated by either metric.

Topham et al. (1983) found evidence that the Dundas Island polynya expanded during periods of spring (strong) tides and froze over during neap (weak) tides after periods of very cold air temperatures. These changes are broadly consistent with the order-of-magnitude variation in the tidal dissipation over the fortnightly and monthly cycles (λ changed by about 1 unit) found in the model solutions. However, given that the rms currents change by about a factor of two over these cycles, the observation is not sufficient to distinguish the relative contributions of the sensible heat and secondary mechanisms.

From the dynamics, it seems reasonable to expect that sensible heat polynyas should freeze later and thaw earlier than the surrounding ocean. For the polynyas identified with tidal forcing, no evidence of this pattern appears in the maps of typical freeze-up and break-up dates published by the Canadian Ice Service (Environment Canada, 2002). However, in the maps of median ice concentration as a function of time of year (Environment Canada, 2002), the polynyas at Hell Gate and Cardigan Strait, Dundas Island, Penny Strait and Queens Channel, and Lambert Channel are evident as areas of low ice concentration compared to the surrounding ocean.

Satellite images are another source of information about ice breakup. A preliminary examination of recent years (Ingrid Peterson, Bedford Institute of Oceanography, pers. comm. 2006) shows early breakup (relative to the surrounding ocean) that corresponds to the polynyas in Hell Gate and Cardigan Strait, Penny Strait and Queens Channel, Dundas

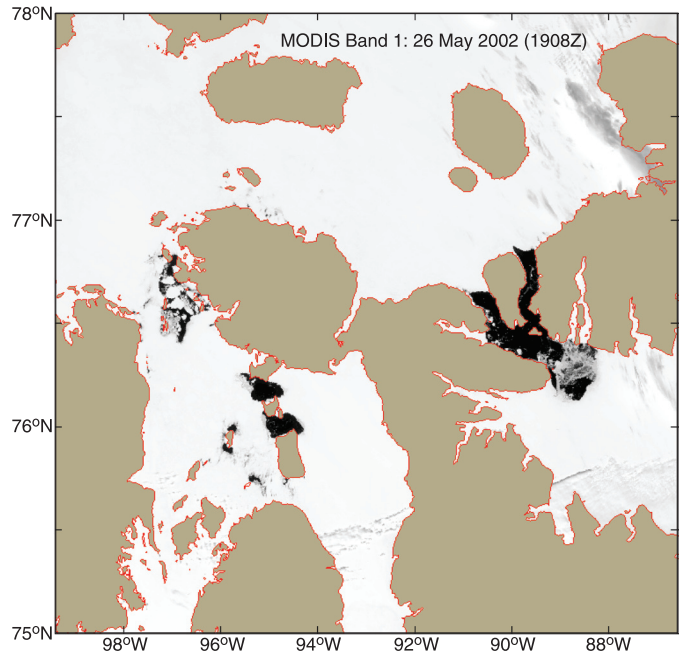


FIG. 10. MODIS satellite image for 26 May 2002 showing open water (dark) in Hell Gate and Cardigan Strait and around the islands in Penny Strait and Queens Channel. Courtesy of Ingrid Peterson (Bedford Institute of Oceanography).

Island (Fig. 10), and Lambert Channel. Figure 10 suggests a connection between the open water and the numerous small islands in the Penny Strait and Queens Channel region. Satellite images also show early breakup around King William Island, where there is some indication of elevated tidal currents. Quantifying the relationship between ice breakup and tidal currents would be a fruitful area for future investigation. In particular, an understanding of whether the relationship is driven by the vertical heat transfer or by mechanical stresses caused by strong tidal currents would provide guidance for future ice modeling.

Limitations

The analysis presented here has several limitations. First, it is local and does not address the important issue of the need for the polynya to be sheltered from drifting ice. Second, we have not addressed the warm water reservoir that is required for the sensible heat mechanism (Melling, 2002). These limitations have not been a serious problem, as a known polynya was identified with every region that had $\lambda < 3$ and a vertical excursion greater than 10 m. A third limitation is that the qualitative analysis does not allow for assessing the relative potential contributions of the different processes. All three of these issues require a much more comprehensive modeling approach than was used here. The focus in this paper has been to define the areas where the tidal currents are likely to make an important contribution to polynya dynamics. These results can be used to help interpret the results of the more comprehensive models.

One limitation of the tidal model fields presented in this paper is that many small features of the tidal currents are not represented. We have already noted the importance of the small spatial scales in relation to Bellot Strait and Penny Strait. The Dundas Island polynya studied by Topham et al. (1983) was also small in relation to the 2–10 km resolution of the tidal model, being only about 1 km across. The archipelago has a complex geometry, with many small islands and channels that can give rise to large tidal currents over small scales. To capture these features would require both higher spatial resolution and a much more extensive mapping of the water depths in the coastal areas.

A second limitation is that all of the model fields are sensitive to the quality of the bathymetry. For example, an artificial sill in a narrow channel will lead to the prediction of larger tidal currents, increased mixing, and larger vertical excursions. In a channel where flow cannot go around obstacles, the errors in the currents scale with the depth h , those in the vertical excursions, with h^2 , and the errors in h/U^3 , with h^4 (Loder and Greenberg, 1986). Thus the derived quantities are very sensitive to depth errors. Detailed bathymetry data have been scarce in the archipelago; over the next few years, however, new bathymetry data sets will result from the data collected by the projects of ArcticNet (www.arcticnet-ulaval.ca), the Canadian component of the International Polar Year (www.ipycanada.ca), and the data recovery efforts of the Canadian Hydrographic Service (Herman Varma, CHS, Bedford Institute of Oceanography, pers. comm. 2007).

A third limitation is that the vertical excursion metric does not predict which water masses (e.g., the bottom or mid-depth waters) are likely to be upwelled. If warm water is not present, then the metric does not provide meaningful information. Some preliminary analysis was done with the temperature and salinity climatology of Kliem and Greenberg (2003), which is based on historical data collected at the Marine Environment Data Service (MEDS) in Ottawa and other sources. This climatology is still too coarse to be useful at the scale of the polynyas. In this area, three-dimensional tidal and circulation models of the archipelago will play a critical role.

Tidal Mixing Fronts and Other Applications

The tidal mixing parameter ($\lambda = \log_{10} h/U^3$) is used in mid-latitude systems to identify the locations of tidal mixing fronts, which are important for productivity at planktonic and higher trophic levels (Backus and Bourne, 1987; Horne et al., 1989). For Georges Bank (Garrett et al., 1978) and the Irish Sea (Simpson and Hunter, 1974), the critical value (λ_c) separating well-mixed from stratified water tends to be about 2. However, the details of the surface heat flux, wind mixing, and horizontal advection of heat and freshwater play an important role in determining λ_c . For example, in the Gulf of California, where λ_c is estimated to be in the range of 2.7 to 3 (Argote et al., 1995), much less mixing is needed to create a well-mixed water column than is needed on Georges Bank.

In the Canadian Arctic Archipelago, the upper ocean stratification in summer is dominated by the freshwater contribution rather than by surface heat fluxes. Observations in Cardigan Strait when λ was about 2.3–2.7 (peak tidal currents of 1 to 1.5 m s⁻¹ in 200 m of water) showed that the water column was not well mixed (Humphrey Melling, Institute of Ocean Sciences, pers. comm. 2005). To assess whether λ is a useful predictor of summer stratification, we computed the average stratification (bottom density minus surface density divided by the water depth) for all of the observations in the compilation of Kleim and Greenberg (2003). While there were hints that weak stratification is associated with small λ , there was not a strong relationship. In addition, there was no evidence of a critical value λ_c where $\lambda < \lambda_c$ implies a well-mixed water column. As expected, processes such as the ice melt cycle and subsequent advection of fresher water (buoyancy) play a dominant role in the stratification.

The fact that areas in Figure 4 with $\lambda < 3$ are not expected to be well mixed in the summer does not necessarily diminish the utility of the map. Enhanced plankton productivity related to tidal mixing does not require that the mixing produce a well-mixed water column; it simply requires that nutrients be mixed into the euphotic zone. In fact much of the enhanced productivity at tidal mixed fronts is in the partially mixed (or transition) zone, not in the well-mixed area (Horne et al., 1989; Kiørboe, 1993; Fig. 29). The areas with $\lambda < 3$ can be thought of as areas where tidal mixing is most likely to matter to plankton productivity in the archipelago. Thus the same tidal processes that contribute to polynya formation in the winter may also contribute to biological productivity in the summer. In addition, Simpson et al. (1982) found that strong tidal currents flowing around islands led to enhanced mixing and high productivity via a mechanism not represented here, so the maps of rms tidal currents may also be useful indicators of enhanced mixing and productivity.

A relationship between the spatial distribution of tidal mixing and the patterns of early human settlement has been suggested for western Sweden (Schmitt et al., 2006). In the Canadian Arctic Archipelago, polynyas are associated with early human settlement patterns (Schledermann, 1980). Schledermann (1978) identified more than 200 prehistoric settlement sites in the area around McDougall Sound (the body of water between Bathurst Island and Cornwallis Island with the Karluk Brooman polynyas at the northern end). Overall, the area between Bathurst Island and Devon Island contains several polynyas where tidal mixing is important. If tidal mixing provides enhanced biological productivity in this area in the summer, then there is additional support for the idea that the area was particularly suitable for early human habitation. The same may be true of other areas in the archipelago with numerous small islands and narrow channels.

Tidal currents can contribute to the vertical transport of heat and nutrients through the generation of internal tides. The one-dimensional internal tide generation function of Baines (1982) can be written:

$$F = \frac{UN^2h'}{\omega h} \quad (2)$$

where N^2 is the Brunt-Vaisala frequency, a measure of stratification; U is the amplitude of the tidal current; $[h']$ is the bathymetric gradient (one-dimensional version of ∇h); ω is the frequency; and terms related to time and vertical position have been ignored. In terms of the vertical excursion, Δz , defined in (1), F can be rewritten

$$F = \Delta z N^2 / h \quad (3)$$

Ignoring N^2 , one can see that F and Δz differ only by h^{-1} and therefore hot spots in Figure 6 are also potential sites for internal tide generation. We leave the detailed mapping of internal tide generation sites, which should include estimates of N^2 , to future work.

CONCLUSIONS

Maps of tidal currents, tidal mixing, and the vertical excursion derived from a tidal model for the Canadian Arctic Archipelago were used to assess the potential contribution of tidal currents to polynya formation and maintenance. The hot spots on these maps support the previous identification of the polynyas at Hell Gate, Cardigan Strait, and Dundas Island as polynyas where tidal forcing makes a substantial contribution to the sensible heat flux. The results also suggest a tidal contribution to the polynyas at Fury and Hecla Strait, Lambert Channel, and Committee Bay, as well as to the Karluk Brooman polynyas among the islands between Cornwallis Island and Bathurst Island at the head of McDougall Sound. The polynyas labeled Lady Ann Strait, Coburg Island, Viscount Melville Sound, Lancaster Sound, and Bylot Island (Fig. 1) were not identified by either metric and appear to be unrelated to tidal forcing, as noted by previous authors (e.g., Barber and Masson, 2007; Smith and Rigby, 1981).

The complex geometry of the Canadian Arctic Archipelago includes many small islands and channels that can give rise to large tidal currents over small scales. The ability of the tidal model to resolve these flows is limited by horizontal resolution (2–10 km in the archipelago) and bathymetric information. These limitations may explain why the tidal metrics failed to identify several known polynyas (e.g., Bellot Strait, Penny Strait, and Queens Channel). New bathymetric measurements from ArcticNet programs (John Hughes Clarke, University of New Brunswick, pers. comm. 2007) and the International Polar Year programs and data recovery by the Canadian Hydrographic Service will lead to improved bathymetry compilations over the next few years. These calculations can then be redone with the new data.

Although the link between the tidal mixing factor (h/U^3) and summer plankton productivity has not been demonstrated in the Canadian Arctic Archipelago, h/U^3 has proven to be a robust predictor of tidal mixing fronts and

enhanced biological productivity in mid-latitude systems. Hot spots of h/U^3 that correspond to polynyas therefore have the potential to be biologically important year-round.

The development of sophisticated coupled ice-ocean models will lead to greater insights and improved descriptions of polynya dynamics in the Canadian Arctic Archipelago. Nevertheless, the conclusions reached in this paper are robust, and the maps of the tidal currents, mixing, and vertical excursion should be useful for many applications.

ACKNOWLEDGEMENTS

We thank Simon Prinsenberg for his support of modeling in the Arctic Archipelago, Brian Petrie and anonymous reviewers for thoughtful and constructive reviews, and Liam Petrie for assistance with the figures. This work was funded in part by the Program for Energy Research and Development (PERD) and in part by NOAA funds through Peter Rhines (University of Washington). C.G. Hannah thanks the Department of Oceanography at Dalhousie University for its support during his professional development leave. The data used in Figure 10 were acquired as part of NASA's Earth Science Enterprise. The algorithms were developed by the MODIS Science Teams. The data, processed by the MODIS Adaptive Processing System (MODAPS) and Goddard Distributed Active Archive Center (DAAC), are archived and distributed by the Goddard DAAC.

APPENDIX A: TIDAL MODEL VALIDATION

The original solutions of Dunphy et al. (2005) were redone after it was found that the water depths were much too shallow in several places including Fury and Hecla Strait and Hell Gate. Hannah et al. (2008) report the complete revalidation of the model results.

Elevation

The highlights of the regional evaluation are given here. The first error metric is the magnitude of the difference between the observed and modeled tidal constituents at a given station,

$$E_C = \left| A_o e^{i\phi_o} - A_m e^{i\phi_m} \right| \quad (4)$$

where A_o , ϕ_o are the observed amplitude and phase and A_m , ϕ_m are the modeled values. E_C combines the amplitude and phase errors into a single metric. The second metric evaluates the quality of the tidal predictions by comparing the predictions made for one year using the observed and modeled constituents,

$$E_T = rms(T_o - T_m) \quad (5)$$

where T_o and T_m are the observed and modeled tidal height time series and rms is the root-mean-square. A normalized version was also calculated:

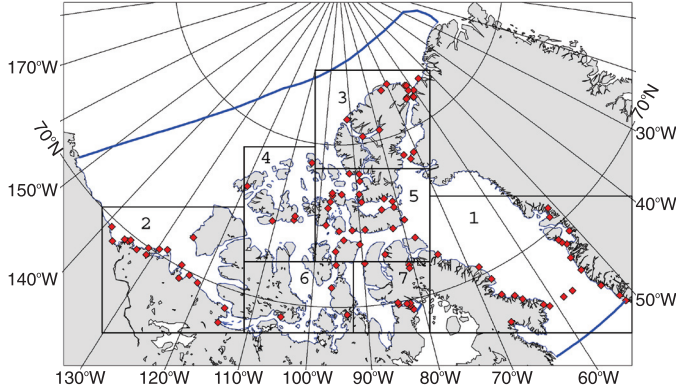


FIG. 11. Map of the Canadian Arctic Archipelago, showing the locations of the tide and pressure gauges (♦) used in the modeling. The boxes labeled 1 to 7 are the regions for which statistics were calculated. The thick lines are the model boundaries.

$$E^*_T = E_T / rms(T_o) \quad (6)$$

Observed time series were compared with the modeled time series based on the five major constituents.

The assimilation loop was run eight times after which the solutions stopped improving. The improvement at the validation stations (not used in the assimilation) was similar to that at the assimilation stations (Table 3 in Hannah et al., 2008). This similarity indicates that the assimilation procedure was not compromising the overall solution in order to improve the simulation at the assimilation stations. The domain-wide errors are reported in the Methods section.

To evaluate the quality of the simulations we computed regional averages of E_C , E_T , and E^*_T using the root-mean-square of the station-by-station values for the regions shown in Figure 11. The largest regional errors (Table 2) are those for the M_2 constituent, which range from 16.3 cm in Baffin Bay, where the M_2 tide is large, to 7.4 cm in the Northwest, where it is smallest. The errors in the other constituents generally range from 1 cm to 7 cm. The exceptions are errors of 10.3 cm for N_2 and 12.6 cm for S_2 in Baffin Bay and an error of 8.5 cm for K_1 in the Southeast. The K_1 error in the Southeast reported by Hannah et al. (2008) is a 10 cm improvement compared to Dunphy et al. (2005) and is the primary improvement resulting from improved bathymetry.

The quality of the tidal predictions is evaluated using E_T and E^*_T . The regional prediction errors range from 6.4 cm to 17.8 cm (Table 3). The regional distribution of the errors is broadly consistent with the M_2 constituent errors. For the normalized prediction errors (under “norm” in Table 3; based on E^*_T), a value of zero means that the modeled time series is identical to the observed one, whereas a value greater than 1 means that using the model prediction is worse than using nothing. The highest-quality solutions are those for the Central and Southeast regions, where the normalized errors are less than 0.3. Baffin Bay and Northwest are of intermediate quality, with normalized errors between 0.4 and 0.5. The North and South Central regions are next, with normalized errors in the range 0.6–0.8. The worst region is West, with normalized errors greater than 0.9 but less than 1.

TABLE 2. Regional comparison of the errors (in cm) for each constituent, calculated using the regional root-mean-square values of E_C . The numbers in the Region column refer to the numbered boxes in Figure 11.

Region	M_2	N_2	S_2	K_1	O_1
1. Baffin Bay	16.3	10.3	12.6	6.9	2.6
2. West	13.7	1.8	3.4	3.8	1.9
3. North	14.7	4.0	6.4	3.7	2.3
4. Northwest	7.4	1.5	3.9	4.8	2.2
5. Central	11.8	2.1	5.3	5.2	2.0
6. South Central	7.6	1.0	2.4	3.4	2.4
7. Southeast	11.4	4.9	5.7	8.5	3.7

TABLE 3. Regional tidal prediction errors. The “cm” column shows the root-mean-square regional values of the station-by-station values of E_T (cm). The “norm” column values are based on E^*_T (dimensionless). The observed and modeled time series were calculated using the five constituents (M_2 , N_2 , S_2 , K_1 , and O_1).

Region	cm	norm
1. Baffin Bay	17.8	0.43
2. West	10.5	0.92
3. North	13.2	0.82
4. Northwest	7.1	0.43
5. Central	10.1	0.25
6. South Central	6.4	0.67
7. Southeast	11.7	0.21

Currents

The comparison of the major axis currents for M_2 and K_1 is shown in Figure 4. The sources of the observations, the names of the station locations, and their latitude and longitude are reported in Table 4. The values of the major axis currents are reported in Table 5.

TABLE 4. The names and locations of the current meter data reported in Figures 3 and 4. The SP1–SP5 data are from Pettipas et al. (2006); HMI–HM3 data are from Humfrey Melling (IOS, pers. comm. 2006); and JS1–JS10 data are from Stronach et al. (1987). SP1 and SP2 cover different parts of the water column and were merged into a single vertical average.

Fig. 3 Label	Name in Source	Latitude (° N)	Longitude (° W)
SP1	BIO1438	74.0834	91.0552
SP2	BIO1439	74.0818	91.0329
SP3	BIO1441	74.3205	90.8511
SP4	BIO1443	74.3205	90.7210
SP5	BIO1445	74.5366	90.4249
HMI	CDG98-54m	76.5331	90.4738
HM2	HLG00-57m	76.5662	89.7600
HM3	CDG00-85m	76.5400	90.3824
JS1	Lancaster-Sound-1	74.0917	81.1667
JS2	Lancaster-Sound-3	74.1233	82.2167
JS3	Wellington-Channel-2	75.265	93.0083
JS4	Wellington-Channel-3	75.2633	92.8500
JS5	Peel-Sound-84	73.6933	96.0000
JS6	Peel-Sound-82	73.6933	96.6167
JS7	Penny-Strait-East	76.6333	96.90000
JS8	Penny-Strait-West	76.6000	97.4167
JS9	Danish-Strait	77.8333	100.7670
JS10	Austin-Channel	75.3833	102.6330

TABLE 5. Comparison of the M_2 and K_1 major axis currents from the observations (Obs) and the model (Model). These are the data reported in Figure 4. The units are cm s^{-1} .

Station	M_2		K_1	
	Obs	Model	Obs	Model
SP1/2	8.9	8.6	9.0	12.0
SP3	8.9	9.4	11.8	12.1
SP4	9.8	9.0	12.2	11.7
SP5	9.3	8.9	10.2	10.5
JS1	3.7	2.7	6.0	5.9
JS2	4.5	2.8	8.2	6.7
JS3	5.8	6.3	9.0	10.0
JS4	6.8	6.6	9.6	10.0
JS5	10.0	9.4	3.1	4.2
JS6	9.0	8.5	2.5	3.6
JS7	18.8	13.5	13.6	12.6
JS8	9.0	15.2	8.1	13.7
JS9	9.1	9.4	4.4	2.1
JS10	5.0	3.1	4.4	5.9
HM1	62	51	35	34.4
HM2	88	62	55	34.1
HM3	66	51	57	34.1

REFERENCES

- Argote, M.L., Amador, A., Lavin, M.F., and Hunter, J.R. 1995. Tidal dissipation and stratification in the Gulf of California. *Journal of Geophysical Research* 100:16103–16118.
- Backus, R.H., and Bourne, D.W., eds. 1987. *Georges Bank*. Cambridge: MIT Press.
- Baines, P.G. 1982. On internal tide generation models. *Deep-Sea Research* 29:307–338.
- Barber, D.G., and Massom, R.A. 2007. The role of sea ice in Arctic and Antarctic polynyas. In: Smith, W.O., and Barber, D.G., eds. *Polynyas: Windows to the world*. Elsevier Oceanographic Series 74. Amsterdam: Elsevier. 1–54.
- Brown, R.G.B., and Nettleship, D.N. 1981. The biological significance of polynyas to Arctic colonial seabirds. In: Stirling, I., and Cleator, H., eds. *Polynyas in the Canadian Arctic*. Occasional Paper Number 45. Ottawa: Canadian Wildlife Service. 59–65.
- Carrère, L., and Lyard, F. 2003. Modeling the barotropic response of the global ocean to atmospheric wind and pressure forcing: Comparisons with observations. *Geophysical Research Letters* 30:1275.
- Daly, S.F. 1994. Evolution of frazil ice in natural bodies of water. In: Daly, S.F., ed. *International Association for Hydraulic Research Working Group on Thermal Regimes: Report on frazil ice*. U.S. Army Corps of Engineers Cold Regions Research and Engineering Laboratory, Special Report 94-23. 11–17.
- Den Hartog, G., Smith, S.D., Anderson, R.J., Topham, D.R., and Perkin, R.G. 1983. An investigation of a polynya in the Canadian Archipelago, 3: Surface heat flux. *Journal of Geophysical Research* 88:2911–2916.
- Dunphy, M., Dupont, F., Hannah, C.G., and Greenberg, D. 2005. Validation of a modelling system for tides in the Canadian Arctic Archipelago. Canadian Technical Report of Hydrography and Ocean Sciences 243. Dartmouth, Nova Scotia: Bedford Institute of Oceanography. vi + 70 p. www.dfo-mpo.gc.ca/Library/316074.pdf.
- Dupont, F., Hannah, C.G., Greenberg, D.A., Cherniawsky, J.Y., and Naimie, C.E. 2002. Modelling system for tides for the Northwest Atlantic Coastal Ocean. Canadian Technical Report of Hydrography and Ocean Sciences 221. Dartmouth, Nova Scotia: Bedford Institute of Oceanography. vii + 72 p. www.dfo-mpo.gc.ca/Library/265855.pdf.
- Dupont, F., Hannah, C.G., and Greenberg, D.A. 2005. Modelling the sea level in the upper Bay of Fundy. *Atmosphere-Ocean* 43:33–47.
- Environment Canada. 2002. *Sea ice climatic atlas – northern Canadian waters, 1971–2000*. Ottawa: Minister of Public Works and Government Services Canada. <http://ice-glaces.ec.gc.ca/under/IceArchive/>.
- Garrett, C.J.R., Keeley, J.R., and Greenberg, D.A. 1978. Tidal mixing versus thermal stratification in the Bay of Fundy and Gulf of Maine. *Atmosphere-Ocean* 16:403–423.
- Hannah, C.G., Dupont, F., Collins, A.K., Dunphy, M., and Greenberg, D. 2008. Revisions to a modeling system for tides in the Canadian Arctic Archipelago. Canadian Technical Report of Hydrography and Ocean Sciences 259. vi + 62 p. www.dfo-mpo.gc.ca/Library/332543.pdf.
- Horne, E.P.W., Loder, J.W., Harrison, W.G., Mohn, R., Lewis, M.R., Irwin, B., and Platt, T. 1989. Nitrate supply and demand at the Georges Bank tidal front. *Scientia Marina* 53:145–158.
- Ingram, R., Bacle, J., Barber, D., Gratton, Y., and Melling, H. 2002. An overview of physical processes in the North Water. *Deep-Sea Research Part II* 49:4893–4906.
- Kjørboe, T. 1993. Turbulence, phytoplankton cell-size, and the structure of pelagic food webs. *Advances in Marine Biology* 29:1072–1093.
- Kliem, N., and Greenberg, D.A. 2003. Diagnostic simulations of the summer circulation in the Canadian Arctic Archipelago. *Atmosphere-Ocean* 41:273–289.
- Loder, J.W., and Greenberg, D.A. 1986. Predicted positions of tidal fronts in the Gulf of Maine region. *Continental Shelf Research* 6:397–414.
- Lynch, D.R., Naimie, C.E., and Hannah, C.G. 1998. Hindcasting Georges Bank circulation, Part 1: Detiding. *Continental Shelf Research* 17:607–639.
- Melling, H. 2002. Sea ice of the northern Canadian Arctic Archipelago. *Journal of Geophysical Research* 107(C11), 3181, doi:10.1029/2001JC001102.
- Morse, B., Ringo, B., Stander, E., Robert, J.-L., Messier, D., and Thanh-Quach, T. 2006. Growth and decay of estuary ice cover. *Journal of Cold Regions Engineering* 20:70–94.
- Ocean and Ecosystem Science, Fisheries and Oceans Canada. 2008. WebTide tidal prediction model. http://www.mar.dfo-mpo.gc.ca/science/ocean/coastal_hydrodynamics/WebTide/webtide.html.
- Padman, L., and Erofeeva, S. 2004. A barotropic inverse tidal model for the Arctic Ocean. *Geophysical Research Letters* 31, L02303, doi:10.1029/2003GL019003.
- Pettipas, R., Hamilton, J., and Prinsenber, S. 2006. Moored current meter and CTD observations from Barrow Strait, 2002–2003. Canadian Data Report of Hydrography and Ocean Sciences 167. Dartmouth, Nova Scotia: Bedford Institute of Oceanography. v + 118 p. www.dfo-mpo.gc.ca/Library/321132.pdf.

- Prinsenber, S.J., and Hamilton, J. 2005. Monitoring the volume, freshwater and heat fluxes passing through Lancaster Sound in the Canadian Arctic Archipelago. *Atmosphere-Ocean* 43: 1–22.
- Saucier, F.J., Senneville, S., Prinsenber, S.J., Roy, F., Smith, G., Gachon, P., Caya, D., and Laprise, R. 2004. Modelling the sea ice–ocean seasonal cycle in Hudson Bay, Foxe Basin and Hudson Strait, Canada. *Climate Dynamics* 23:303–326.
- Schledermann, P. 1978. Prehistoric demographic trends in the Canadian High Arctic. *Canadian Journal of Archaeology* 2: 43–58.
- . 1980. Polynyas and prehistoric settlement patterns. *Arctic* 33:292–302.
- Schmitt, L., Larsson, S., Schrumm, C., Alekseeva, I., Tomczak, M., and Svedhage, K. 2006. ‘Why they came’: The colonization of the coast of western Sweden and its environmental context at the end of the last glaciation. *Oxford Journal of Archaeology* 25:1–28.
- Simpson, J.H., and Hunter, J.R. 1974. Fronts in the Irish Sea. *Nature* 250:404–406.
- Simpson, J.H., Tett, P.B., Argote-Espinoza, M.L., Edwards, A., Jones, K.J., and Savidge, G. 1982. Mixing and phytoplankton growth around an island in a stratified sea. *Continental Shelf Research* 1:15–31.
- Smith, M., and Rigby, B. 1981. Distribution of polynyas in the Canadian Arctic. In: Stirling, I., and Cleator, H., eds. *Polynyas in the Canadian Arctic*. Occasional Paper Number 45. Ottawa: Canadian Wildlife Service. 7–19.
- Smith, S.D., Anderson, R.J., Den Hartog, G., Topham, D.R., and Perkin, R.G. 1983. An investigation of a polynya in the Canadian Archipelago, 2: Structure of turbulence and sensible heat flux. *Journal of Geophysical Research* 88(C5):2900–2910.
- Smith, S.D., Muench, R.D., and Pease, C.H. 1990. Polynyas and leads: An overview of physical processes and environment. *Journal of Geophysical Research* 95:9461–9479.
- Smith, W.O., and Barber, D.G., eds. 2007. *Polynyas: Windows to the world*. Elsevier Oceanographic Series 74. Amsterdam: Elsevier. 458 p.
- Stirling, I. 1980. The biological importance of polynyas in the Canadian Arctic. *Arctic* 33:303–315.
- . 1981. Introduction. *Polynyas in the Canadian Arctic*. In: Stirling, I., and Cleator, H., eds. *Polynyas in the Canadian Arctic*. Occasional Paper Number 45. Ottawa: Canadian Wildlife Service. 5–6.
- Stirling, I., and Cleator, H., eds. 1981. *Polynyas in the Canadian Arctic*. Occasional Paper Number 45. Ottawa: Canadian Wildlife Service. 70 p.
- Stronach, J.A., Helbig, J.A., Salvador, S.S., Melling, H., and Lake, R.A. 1987. Tidal elevations and tidal currents in the Northwest Passage. Canadian Technical Report of Hydrography and Ocean Sciences 97. 346 p. www.dfo-mpo.gc.ca/Library/108629.pdf.
- Tang, C.L., and Fissel, D.B. 1991. A simple ice-ocean coupled model for ice drift in marginal ice zones. *Journal of Marine Systems* 2:465–475.
- Topham, D.R., Perkin, R.G., Smith, S.D., Anderson, R.J., and Den Hartog, G. 1983. An investigation of a polynya in the Canadian Archipelago, 1: Introduction and oceanography. *Journal of Geophysical Research* 88(C5):2888–2899.
- Williams, W.J., Carmack, E.C., and Ingram, R.G. 2007. Physical oceanography of polynyas. In: Smith, W.O., and Barber, D.G., eds. *Polynyas: Windows to the world*. Elsevier Oceanographic Series 74. Amsterdam: Elsevier. 55–86.